

## Supplementary Information

### Radical-mediated proton transfer enables hydroxyl radical formation in charge-delocalized water

Ruijuan Zhao <sup>a ‡</sup>, Qiuyue Zhang<sup>b ‡</sup>, Na Yang<sup>c</sup>, Lei Li<sup>a</sup>, Zhenyu Li<sup>b,\*</sup> and Chunhua Cui<sup>a,\*</sup>

<sup>a</sup>Molecular Electrochemistry Laboratory, Institute of Fundamental and Frontier Sciences, University of Electronic Science and Technology of China, Chengdu 611731, China.

<sup>b</sup>Key Laboratory of Precision and Intelligent Chemistry, University of Science and Technology of China, Hefei 230026, China.

<sup>c</sup>School of Materials and Energy, University of Electronic Science and Technology of China, Chengdu, 610054, China.

\*E-mail: zyli@ustc.edu.cn; chunhua.cui@uestc.edu.cn

‡These authors contribute equally

#### **This file includes**

Materials and Methods  
Figures S1 to S6

## Materials and Methods

**Reagents.** KI ( $\geq 99.99\%$ , metals basis), I<sub>2</sub> (99.995%, metals basis), CuCl<sub>2</sub> ( $> 99.9\%$ , AR), 18-Crown-6 ( $> 99.9\%$ ), vitamin C ( $> 99.9\%$ ) were purchased from Aladdin. HCOOK ( $\geq 99.9\%$ ), KIO<sub>3</sub> ( $\geq 99.9\%$ ), and K<sub>2</sub>SO<sub>3</sub> ( $\geq 99.9\%$ ) were purchased from Adamas. High-purity Cu foils ( $> 99.999\%$ ). Isotopically labeled D<sub>2</sub>O ( $> 99.9\%$ ), and D<sub>2</sub>SO<sub>4</sub> ( $> 99.9\%$ ) were purchased from Sigma-Aldrich. Hydrogen peroxide (H<sub>2</sub>O<sub>2</sub>, GR, 30 wt. % in H<sub>2</sub>O, Chron Chemical Co., Ltd.), 2,2,6,6-tetramethyl-1-piperidinyloxy (TEMPO, AR,  $> 99\%$ , Meryer), H<sub>2</sub><sup>17</sup>O (<sup>17</sup>O  $> 90$  atom %, Reertech), H<sub>2</sub><sup>18</sup>O (<sup>18</sup>O  $> 99$  atom %, Energy Chemical). All the H<sub>2</sub>O solutions were prepared using ultrapure water (HPLC Plus, Sigma-Aldrich), Ar (6.0 purity, Linde) and O<sub>2</sub> (4.5 purity, Linde) were used for purging the electrolytes. Hydrochloric acid (HCl) aqueous solution were prepared by high-purity HCl (38%, GR). The solution pH has been adjusted by as-prepared HCl aqueous solution. The solution pH was measured using a glass-electrode pH meter (Starter 2100) calibrated with standard buffer solutions and operating temperatures.

**Electron paramagnetic resonance spectroscopy.** Electron paramagnetic resonance tests were implemented by a Continuous-Wave (CW) spectrometer (Bruker EMX micro) operating in X-band mode with a frequency of 9.848 GHz. Each spectrum was recorded using the following parameters. Briefly, microwave power of 20 mW and modulation amplitude of 1.0 G was applied. 50 mM BMPO (Dojindo) and 100 mM DMPO (Dojindo) were selected as spin-trapping agents. EPR simulations were performed according to the hyperfine splitting constants of the radicals. Temperature-dependent EPR spectra were recorded on a CW-EPR spectrometer equipped with a quartz vacuum dewar cryostat. The detailed instrumental parameters were as follows: central field is 3355 G, scanning width is 200 G, scanning power is 20 mW, scanning time is 300 s, and modulation amplitude is 1.0 G. For temperature EPR measurements, a quartz vacuum dewar cryostat equipped with an electrical heater and liquid nitrogen gas was required to maintain the corresponding test temperature. The EPR data was collected at the indicated temperature.

**High-resolution mass spectrometry.** The compounds were identified using a quadrupole time-of-flight mass spectrometry (Waters XEVO G2-XS QTof) by positive APCI and ESI ion source mode. For the preparation of 18C6-cations solution, 18C6 has been added into isotope-labelled H<sub>2</sub>O, H<sub>2</sub><sup>18</sup>O and D<sub>2</sub>O solutions, respectively. Then the solution pH was adjusted with HCl to 1.5. The aqueous solutions were pre-purged with Ar for at least 30 min while implemented in Ar

atmosphere afterwards.

**UV-Vis spectroscopy.** The UV-vis spectroscopy was implemented on a QE Pro UV-visible spectrometer (Ocean Optics) equipped with an HL-2000 light source and a DH-2000-BAL light source (200 to 950 nm). A fibre-optic cable (100  $\mu\text{m}$  fibre core diameter) was used for the light path through the sample to the detector. The aqueous solutions were always pre-purged with Ar for at least 30 min. The Cu foils were immersed in HCl solutions with different pH values. After one day of operation, the resultant solution containing dissolved  $\text{Cu}^{2+}$  was used for UV-Vis measurements. Similarly, the mixtures of 20 mM KI with different pH of HCl solutions were evaluated with UV-Vis spectroscopy. The baselines were obtained with pure water as a background.

**Material characterizations.** The surface corrosion of the resultant Cu foils was observed by a field-emission scanning electron microscope (SEM, ZEISS Sigma 300). Before SEM, the Cu foils were cleaned with deionized water and dried with Ar-flowing gas. A Bruker M4 Tornado X-ray fluorescence (XRF) with a Ru target was used to determine the dissolved  $\text{Cu}^{2+}$  ( $\text{Cu-K}\alpha$ ) content in HCl aqueous solutions by dropping  $\text{Cu}^{2+}$ -containing HCl solutions onto the carbon papers.

**Molecular dynamics (MD) simulations.** All simulations were performed using density functional theory (DFT) implemented in CP2K. The hybrid B3LYP functional was used with a dispersion correction (B3LYP-D3). Goedecker–Teter–Hutter (GTH) norm-conserved pseudopotentials were used together with the DZVP basis set combined with an auxiliary planewave basis set. An energy cutoff of 400 Ry was imposed for the plane wave basis set, and a 40 Ry cutoff was used for the grid at which a Gaussian basis function was mapped. The NVT ensemble was realized by a Nose–Hoover chain thermostat at 298.15 K. AIMD simulations performed in a periodic box of 64 water molecules were run for 20 ps and the time step was set to be 1 fs. One electron was removed by changing the total charge of the system and added a  $\text{H}_3\text{O}^+$  ion when simulating the  $\text{H}_2\text{O}^+$ -mediated proton transfer process. In the HCl aqueous solution, we additionally added a  $\text{H}_3\text{O}^+$  ion and a  $\text{Cl}^-$  ion. Hirshfeld charges were calculated using CP2K. The net charge of each molecule was obtained by counting the sum of the net charges of hydrogen and oxygen atoms in each molecule. The hydrogen-bonded configurations were identified by applying a cutoff on the oxygen-oxygen distance  $r_{OO}$  of 3.5 Å and a cutoff on the

hydrogen bond angle  $\angle_{\text{HOO}}$  of  $30^\circ$ .

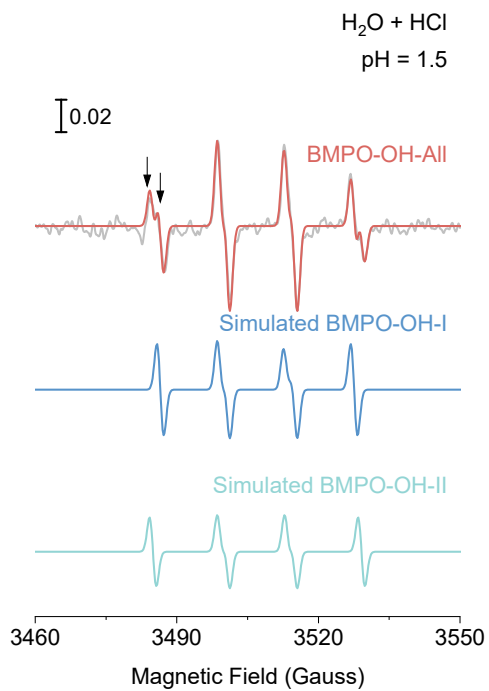


**Figure S1** EPR spectra of BMPO-OH-I and BMPO-OH-II at pH 1.5. Marked arrows show the overlay of BMPO-OH-I and BMPO-OH-II.

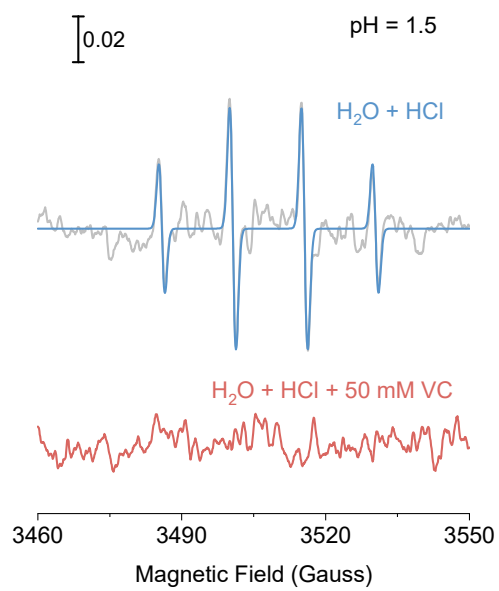


**Figure S2** EPR spectra of DMPO-OH in HCl aqueous solution at pH 1.5 with and without 50 mM VC.

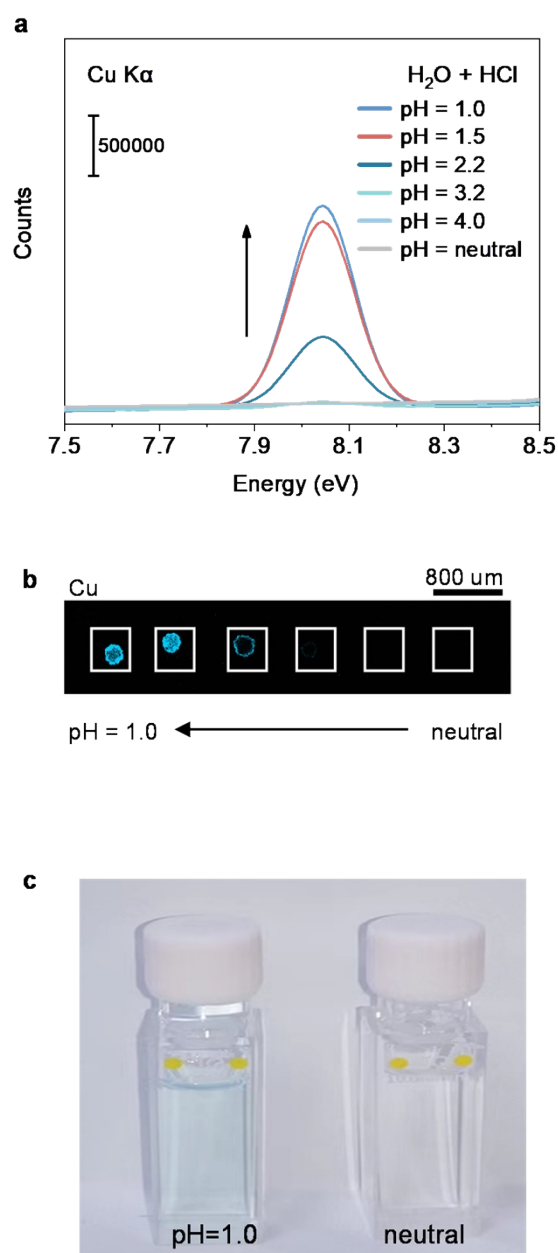


**Figure S3 (a, b)** X-ray fluorescence was used to determine the content of Cu in HCl aqueous solutions with pH adjusted from neutral to 1.0. **(c)**, after 24 hours of corrosion in the Ar pre-purged HCl aqueous solution at pH 1.0, the solution becomes light blue relative to that at neutral condition.

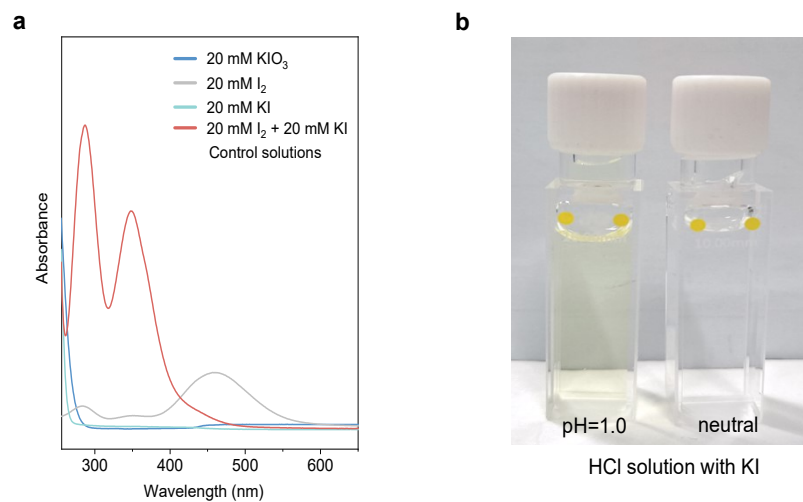


**Figure S4 (a)**, UV-Vis spectra of I-based species. **(b)**, the color change of the Ar pre-purged HCl solutions with pH adjusted from neutral to 1.0 after adding 20 mM KI.

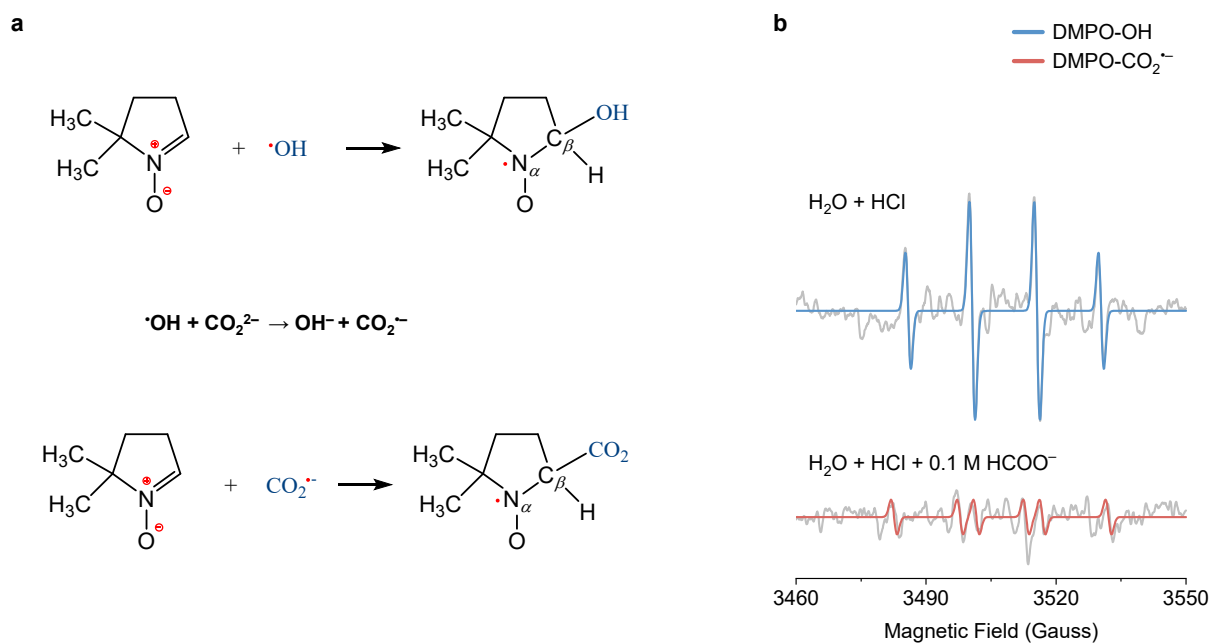


**Figure S5 (a)**, The formation of the DMPO-OH adduct and the DMPO-CO<sub>2</sub><sup>•-</sup> adduct. **(b)**, EPR spectra of DMPO-OH and DMPO-CO<sub>2</sub><sup>•-</sup> in HCl solution at pH=1.5 and after adding 0.1 M HCOOK.

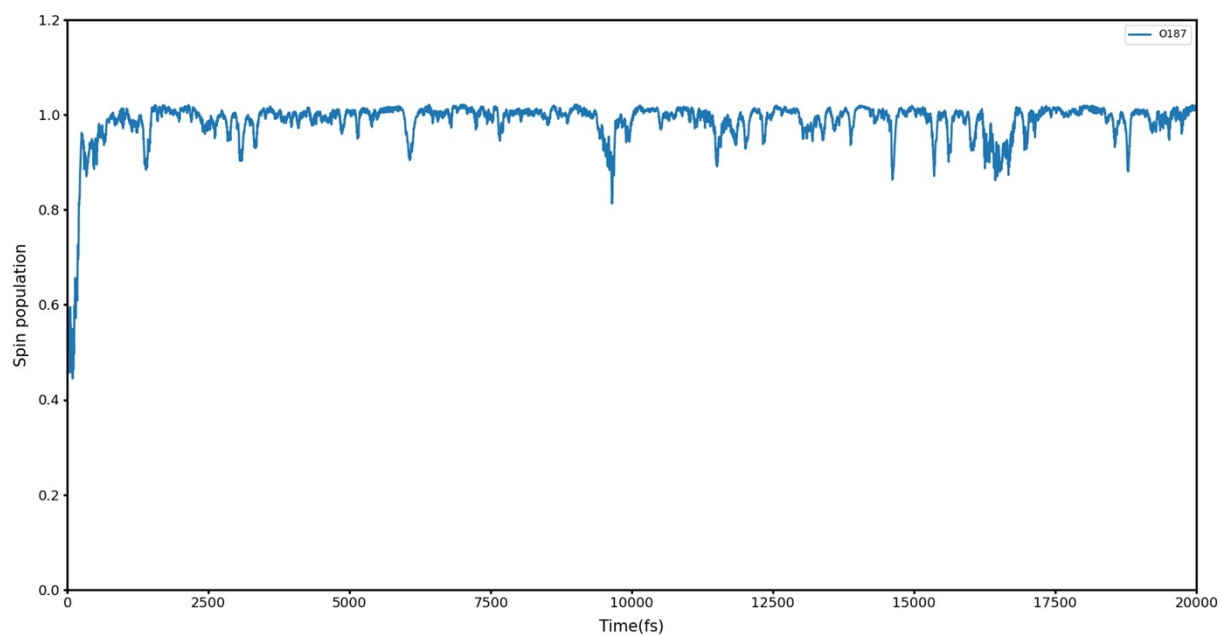


**Figure S 6** The time evolution of the Mulliken spin population on the oxygen atom of the radical. From Movie S1, we can see a radical change from  $\text{H}_2\text{O}^{*+}$  to  $\cdot\text{OH}$ .